International Journal of Computational Methods
Vol. 9, No. 2 (2012) 1240025 (28 pages)

DOI: 10.1142/S0219876212400257

MODELING AND SIMULATION OF MICRO-SCALE WIND FARMS USING HIGH PERFORMANCE COMPUTING

ASHRAF S. HUSSEIN*

Faculty of Computer and Information Sciences
Ain Shams University, Cairo 11566, Egypt
ashrafh@acm.org
http://member.acm.org/∼ashrafh

HISHAM E. EL-SHISHINY

IBM Centre for Advanced Studies in Cairo
IBM Cairo Technology Development Centre
IBM WTC, Egypt Branch, P.O.B. 166
El-Ahram, Giza, Egypt
shishiny@eg.ibm.com

Received 16 May 2011
Revised 7 September 2011

Onshore wind farms usually consist of numerous horizontal axis wind turbines closely placed in clusters, and they are often cited on complex terrain. This paper proposes a computational framework for modeling and simulation of wind flow over micro-scale (and early meso-scale) wind farms using distributed memory, massively parallel high performance computing platforms. The present framework uses the Reynolds Averaged Navier–Stokes (RANS) to model the wind flow over the wind farms, as the flow is considered to be fully turbulent, isothermal and incompressible. The wind turbines installed in the wind farm are modeled by the virtual blade model (VBM). This technique considers the presence of a wind turbine's rotor implicitly through momentum sources placed in an actuator disc, yielding indirectly a pressure jump across the disk, which varies with its radius and azimuth. The nonlinear, aerodynamic interaction between the rotor wakes with each other and with the terrain of the wind farm is simulated by coupling the VBM with the governing flow field equations. In this manner, an efficient parallel algorithm for implementing the VBM was developed and integrated with parallel computational fluid dynamics (CFD) core simulation engine. The accuracy and performance of the proposed framework were confirmed through several test cases carried out on the IBM Blue Gene ultra-scale supercomputer.

Keywords: Horizontal axis wind turbines; wake interactions; micro-scale wind farms; virtual blade model; CFD modeling; high performance computing.

*Corresponding author.

1. Introduction

The world's primary energy needs are projected to grow by 56% between 2005 and 2030, by an average annual rate of 1.8% per year [International Energy Agency (2007)]. In the renewable energy sector, wind power represents one of the most mature technologies. To make wind power economically feasible, it is crucial to optimize wind energy conversion into mechanical energy. Of all the different aspects involved, rotor aerodynamics is a key determinant for achieving this goal [Şahin (2004)]. The operation of Wind Turbine (WT) in a wind farm unavoidably affects the others in its vicinity due to velocity deficit and increased level of turbulence in its wake, reducing the power output and increasing the dynamic loading on the WTs. Wind farms are often placed as close as possible to each other in clusters because of land use restrictions causing WT wakes to interact and contribute more to power losses and dynamic loads. In gross energy production, the losses are estimated to vary from 5% to more than 15% due to wakes, depending on the wind farm layout [Sørensen *et al.* (2007); Zahle and Sørensen (2007); Makridis and Chick (2009)]. Thus, understanding the factors affecting wake characteristics is essential for the optimal sitting of such wind farm, especially when its terrain is complex.

Three approaches are available to analyze the flow field within a wind farm: Field testing, which provides accurate results at selected positions, but is highly complicated and expensive; analytical and semi-empirical models, which adopt simplifying assumptions and are thus not universally reliable; and CFD, which offers the best alternative to direct measurements [Crespo *et al.* (1999); Vermeer *et al.* (2003); Şahin (2004); Jimenez *et al.* (2007); Palma *et al.* (2008); Sumner *et al.* (2010)].

The methodology of wind resource assessment (e.g., [Troen and Petersen (1989); Wind Resource Assessment Handbook (1997)]) has relied on a combination of field data and software tools based on statistics and linear models (e.g., WAsP [Sandström (1994)] and AVENU [Lissaman *et al.* (1989)]). These linear models are based on the concept of linearized flow models originally introduced by [Jackson and Hunt (1975); Mason and Sykes (1979)]. This practice has proved its suitability in the case of relatively flat terrain, being able to resolve both the upwind and the flow at the summit of isolated hills of moderate slope (e.g., [Landberg *et al.* (2003); Ayotte and Hughes (2004)]). However, micro-scale (and early meso-scale) wind farms tend to be installed in terrains of increasing complexity, where the corresponding flow structure is sophisticated, especially when wind turbines are placed very close together in small clusters. In such situations, the linear models are not appropriate and CFD is more useful [Palma *et al.* (2008)].

Research on the aerodynamics of wind turbines is fundamentally concerned not only with the prediction of rotor performance, but also the study of its wake. For many years, the blade element momentum theory (BEM), has been the most popular model for load and performance predictions for wind turbines [Manwell *et al.* (2002); Hansen (2003); Ingram (2005); Lanzafame and Messina (2007)]. Although the BEM method is one of the key methods used routinely in industry, a wide variety

of advanced aerodynamic methods has been developed [Sumner *et al.* (2010)]. Generally, these methods range from actuator-disk (AD) models requiring the use of tabulated airfoil data [Hansen (2003); Mikkelsen (2003)] to models based on the solution of the full unsteady 3-D Navier–Stokes [Ekaterinaris (1997); Duque *et al.* (1999); Xu and Sankar (1999); Xu and Sankar (2000); Sørensen and Michelsen (2000); Benjanirat *et al.* (2003); Mandas *et al.* (2006)].

An extensive overview on different wake modeling methods was presented by Crespo *et al.* [1999], and Vermeer *et al.* [2003] conducted a more up-to-date assessment of the latest research on WT wakes. Most of the simple (kinematic) models, which are commonly used, have been validated for flat terrain cases. A more recent reviews of the different models used for wake modeling have recently been published by Ivanel [2009] and Sanderse *et al.* [2011]. To reduce the computational requirements for wake simulations, the presence of the blades is generally considered with one of three main methods; AD [Madsen (1982); Rajagopalan and Fanucci (1985); Sørensen and Myken (1992); Masson *et al.* (1997); Mikkelsen (2003); Ivanell (2009)], actuator line (AL) [Sørensen and Shen (2002); Troldborg *et al.* (2007); Ivanell (2009)] and actuator surface (AS) [Dobrev *et al.* (2007); Sumner *et al.* (2010); Sanderse *et al.* (2011)]. The more expensive AL and surface techniques use more aerodynamic characteristics of the blade than the AD, and consequently they are more accurate. However, the AD remains the most widely used method for multiple wake simulations because it is easy to implement, achieves good accuracy and consumes lower computational effort [Sumner *et al.* (2010)]. Although still based on the AD model, their computation of the flow field is carried out using Euler, Navier–Stokes or reynolds-averaged Navier–Stokes (RANS) equations, in the work of [Masson *et al.* (2001); Ammara *et al.* (2002); Vermeer *et al.* (2003); Makridis and Chick (2009)].

This work aims at computationally model the micro-scale (and early meso-scale) wind farms using CFD techniques. The atmospheric boundary layer flow over the wind farms is modeled using the RANS equations along with the k–ε model for turbulence closure. The wind turbines' rotors are implicitly considered, within the flow field, by the virtual blade model (VBM), which was originated by Zori *et al.* [1995] and Yang *et al.* [2000]. This model is considered one of the best choices for modeling several wind turbines in micro-scale (or early meso-scale wind farm) from computational cost and fidelity points of view [Sørensen and Shen (2002)]. In this model, the rotor system is replaced by momentum sources placed in an actuator disc, yielding indirectly a pressure jump across the disk, which varies with its radius and azimuth. Thus, the time-averaged effects of the blades are accounted for in the model, without them being present in the computational mesh.

The current implementation of the VBM into a general purpose CFD addresses several shortcomings to most of the previous models. The VBM allows for the specification of rotor blades varying in twist, chord and airfoil type along the span. The rotor forces are determined using the improved BEM theory [Lanzafame and Messina (2007)], using airfoil lookup tables, i.e., lift and drag coefficients versus

angle of attack, can further be specified as functions of Mach and Reynolds numbers, allowing both incompressible and compressible flows to be treated accurately. Furthermore, the VBM allows many different rotors to be treated simultaneously, thus allowing a comprehensive simulation of a wind farm. In this manner, it is achievable to simulate the interaction between the wind turbines, in addition to the terrain of the wind farm, irrespective of its complexity.

The overall simulation and visualization pipeline of [Hussein and El-Shishiny (2009)] was adopted and customized as shown in Fig. 1. The solid model of the wind farm terrain and the turbines specifications and locations are the primary inputs to this pipeline. As the simulation problem is computationally intensive, an efficient parallel algorithm for the proposed VBM was developed and integrated with the Code_Saturne parallel CFD solver [Archambeau *et al.* (2004); Code_Saturne (2010)]. The IBM Blue Gene/L high performance computing (HPC) system [Blue Gene Literature (2009)] was used in this research work, as it is an ultra-scale computer, which has been very effective in addressing these classes of challenging CFD problems with several millions of computational mesh cells. Following this, the whole framework is ported and optimized for EUMEDGRID e-Infrastructure to carry out real simulations, for decision-making purposes, through the grid interface provided by the Egyptian Universities Network, the Egyptian partner in EUMEDGRID-Support Project [EUMEDGRID-Support Project (2011)].

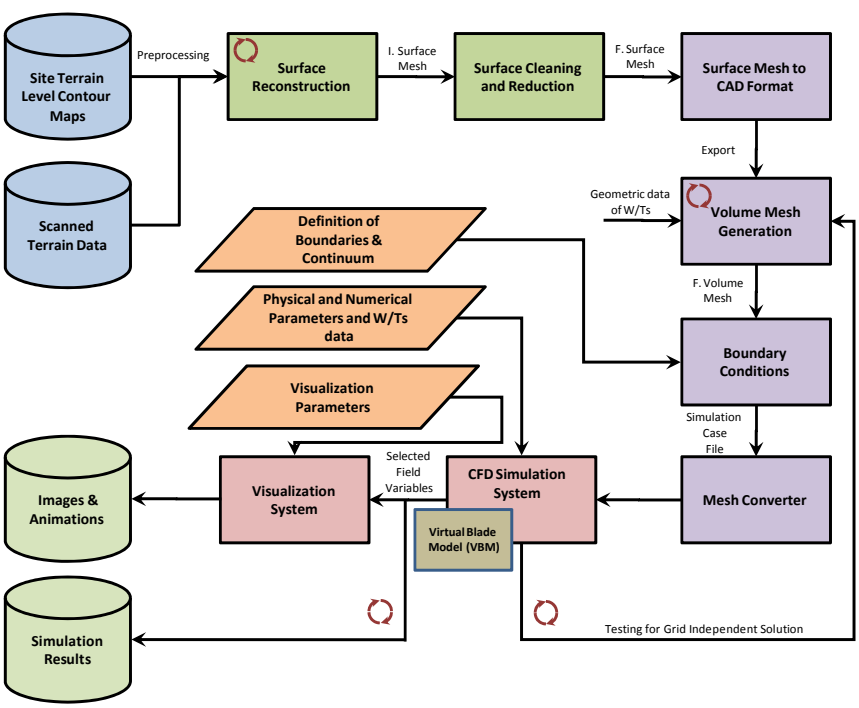

Fig. 1. General simulation and visualization pipeline.

The outline of the rest of the paper is as follows: The nature and characteristics of the problem we intended to solve and the formulation of the model are stated and illustrated in Sec. 2. The simulation setup is outlined in Sec. 3. The results and discussions are presented in Sec. 4. Finally, Sec. 5 gives the conclusion of this work and the future work directions.

2. Model Formulation

2.1. *Wind flow model*

The wind environment over micro-scale (and early meso-scale) wind farms is governed by the conservation laws of mass and momentum. The flow is assumed to be three-dimensional, incompressible Newtonian fluid with constant density. Since this work mainly deals with the prediction of the statistically steady mean flow and turbulence in wind farm environments for situations with neutral stratification, the RANS equations are employed considering the k–ε turbulence models [Archambeau *et al.* (2004)]. The model constants for atmospheric flow are (C_μ, σ_k, σ_ε, $C_{\varepsilon 1}$, $C_{\varepsilon 2}$) = (0.03, 1.00, 1.30, 1.21, 1.92) [Sørensen (1995)].

The bottom boundary was modeled by a rough surface [Menter (1993)]. In the first control volume above the surface, wall laws were applied based on the relationships $k_{\text{wall}} = u_*^2/C_\mu^{0.5}$ and $\varepsilon_{\text{wall}} = u_*^3/[\kappa(z + z_0)]$, where $\kappa = 0.40$ is the von Kármán constant, u_* is the friction velocity and z is the distance above the surface with characteristic roughness height z_0. For inlet boundary condition, a logarithmic boundary layer is developed with height $\delta = 1000$ m. The turbulence kinetic energy (k) and dissipation rate (ε) at the inlet were determined as follows [Palma *et al.* (2008)]:

$$k = \frac{\ell_m^2}{C_\mu^{0.5}} \left(\frac{u_*}{\wp}\right)^2 \quad \text{and} \quad \varepsilon = \ell_m^2 \left(\frac{u_*}{\wp}\right)^3 \tag{1}$$

where $\boldsymbol{\ell}_m = \min[\kappa(z + z_0), C_\mu \delta]$ and $\wp = \kappa(z + z_0)$ if $z \prec \delta$ or $\wp = \delta$, if $z \geq \delta$.

The relationship between the inflow turbulence and the terrain roughness height can be stated as [Cabezón *et al.* (2009)]:

$$z_o = z_{\text{hub}} e^{-0.9895/TI_{\text{in}}} \tag{2}$$

where z_{hub} is the wind turbine-hub height and TI_{in} is the inflow turbulence intensity at turbine-hub height.

At the outflow boundary, constant static pressure was used [Hargreaves and Wright (2007)]. As the top boundary was placed far away outside the boundary layer, symmetry boundary conditions were applied to enforce a parallel flow. At the lateral boundaries, symmetry boundary conditions were also used [Hargreaves and Wright (2007)].

Code_Saturne version 1.4 [Archambeau *et al.* (2004); Code_Saturne (2010)] was used in the present work as a CFD solver. The core simulation engine solves the

turbulent RANS equations for incompressible flows with a fractional time-step method, based on a prediction-correction algorithm for pressure/velocity coupling and a momentum interpolation, to avoid pressure oscillations. The second order Upwind difference scheme is used along with flux reconstruction for spatial discretization [Archambeau *et al.* (2004)]. The simulation requires iterating the solution of the fluid flow equations, starting from an initial guess, until it converges. In this work, a reduction of the residuals of at least six orders of magnitude was used as convergence criteria.

2.2. *Modeling of wind turbines*

For horizontal-axis wind turbines (HAWTs), the VBM models the effect of the rotor in the flow field implicitly through source terms in the momentum equations placed in a cone volume swept by the spinning rotor. This cone is defined by a base radius $R\cos\gamma$, where R is the blade length and γ is the coning angle of the blades as shown in Fig. 2(a). The simulation problem requires us to address two tasks: (a) solving the flow field of the rotor; (b) developing relations for the evaluation of the rotor blade source terms. Here, the flow field is solved using the general purpose CFD solver Code_Saturne. Thus, we are left with the appropriate formulation and implementation of item (b). The source terms representing the rotor, unknown at the start of iterations, evolve as part of the solution. The blade source terms are evaluated using the improved BEM theory [Lanzafame and Messina (2007)], requiring the discretization of the rotor into span-wise elements. Here, we allow the blade properties, such as chord length, c, airfoil type and twist angle, β, to vary over the span of the blade. To calculate the blade source terms, the computed velocity field is used to obtain the local angle of attack, α, and the Reynolds number, Re, at each blade element. A lookup table corresponding to the considered blade section is used to get the local c_L and c_D values, which are corrected for the three-dimensional

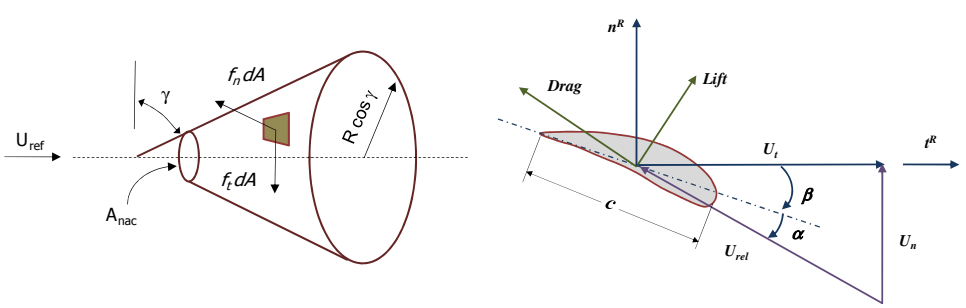

(a) Actuator disk representation of a wind turbine.

(b) Cross-section of a blade.

Fig. 2. WT geometry.

effects [Lanzafame and Messina (2007)]. Then, the instantaneous sectional rotor forces can be calculated in the form:

$$f_{L,D} = \frac{1}{2}\rho U_{\text{rel}}^2 c(r/R) c_{L,D}(\alpha, \text{Re}) \tag{3}$$

The rotor is composed of B blades having a rotational velocity Ω. The x-axis is defined as the turbine's axis of rotation. The forces due to lift and drag over a blade section at a given radial position are presented in Fig. 2(b). In the plane of the section, the fluid velocity relative to the blade, U_{rel}, is decomposed into a normal component U_n and a tangential component U_t.

$$U_{\text{rel}} = \sqrt{U_n^2 + U_t^2}, \quad U_n = -u_i n_i^R, \quad U_t = \Omega r - u_i t_i^R \tag{4}$$

where u_i is the ith fluid velocity fluid velocity component and n_i^R and t_i^R are the appropriate cosine directors of the unit vectors $n^R$and t^R, respectively. The geometric angle of attack is generally defined according to the relationship:

$$\alpha = \arctan\left(\frac{U_n}{U_t}\right) - \beta \tag{5}$$

For the time-averaged solution, only a fraction of these forces must be considered. Assuming constant rotational speed of the rotor, time averaging over one period is identical to geometric averaging over an angle of 2π. Thus, the local resultant forces per cell become:

$$F_{L,D\text{cell}} = B\frac{\Delta r \cdot r\Delta\phi}{2\pi r} \cdot f_{L,D} \tag{6}$$

with r and ϕ being the span-wise and the azimuthal coordinates, respectively. This generalized implementation permits the mesh topology to be either structured or unstructured, allowing both hexahedral and prismatic elements. The above force vector is transformed back into the flow-field reference frame. Then,

$$\vec{S}_{\text{cell}} = -\frac{\vec{F}_{\text{cell}}}{V_{\text{cell}}} \tag{7}$$

is the time-averaged local source term that has to be added to the momentum equations. In the present work, these source terms, Eq. (7), are computed at the corresponding mesh cells within the cone volume swept by the spinning rotor in a fashion shown in Fig. 3. Finally, the flow-field is updated and the iterative procedure is repeated until convergence is attained.

The BEM method can be applied only when the geometry of the blade is given. If such information is not available, it is still possible to represent the rotor's effect on the flow field using the constant loading actuator disc method (ADM). In this

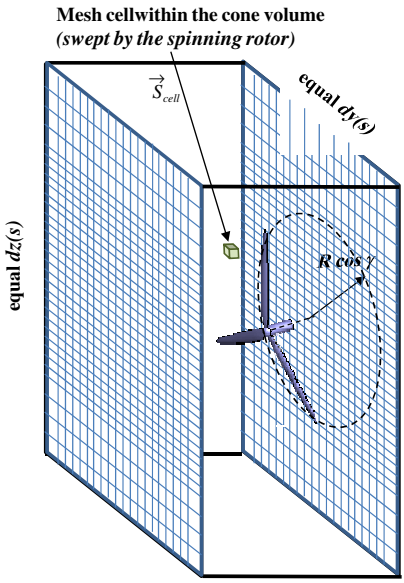

Fig. 3. The source terms representing the turbine's rotor.

manner, the rotor's thrust coefficient is defined as:

$$C_T = \frac{T}{\frac{1}{2}\rho U_{\text{ref}}^2 \pi R^2 \cos^2 \gamma} \tag{8}$$

where πR^2 is the rotor area and T is the total thrust. Assuming that the rotor is uniformly loaded, the normal and tangential components of the surfacing force exerted by the rotor on the flow are:

$$f_n^R = \frac{1}{2}\rho U_{\text{ref}}^2 C_T, f_t^R = 0 \tag{9}$$

For a turbine facing undisturbed stream, the reference velocity U_{ref} is evidently U_∞, but for a turbine in the wake of an upstream turbine or in complex terrain this is not the case. Many approaches were recommended in [Sanderse *et al.* (2011)] to obtain the reference velocity. In this work, an iterative procedure is used starting with an initial value for U_{ref}, from which the axial induction a follows, and then a new reference velocity based on the local flow field is computed as: $U_{\text{ref}} = U_{local}/(1-a)$. This procedure is repeated until convergence is achieved.

The characteristics of the flow past the nacelle depend very strongly on various parameters such as the nacelle's shape, and the flow's orientation, speed and properties. This study aims to simulate the time-averaged aerodynamic response of the complete turbine. Therefore, the nacelle's effects on the flow have been introduced into the formulation in similar fashion to those of the rotor: The nacelle is represented as a disk permeable surface A_{nac} and delimited by a diameter D_{nac} on

which a drag force acts upon the incoming fluid flow. The drag coefficient of bluff bodies of shape similar to typical nacelles varies between 0.8 and 1.2 [El-Kasmi and Masson (2008)]. Consequently, the normal surficial force exerted by the nacelle on the flow is:

$$f_n^{\text{nac}} = \frac{1}{2}\rho U_{\text{ref}}^2 C_{D_{\text{nac}}} \tag{10}$$

2.3. *Implementation of the Virtual Blade Model (VBM)*

The VBM algorithm was designed to be integrated with any parallel CFD solver that can be executed on a distributed computing environment and supports user defined functions or subroutines. The VBM algorithm is comprised of two main parts: (a) The initialization part, which is executed once at the start of computations as described in the following steps 1–4; (b) the iterative part, which is executed consecutively along with the iterations of the flow field solution and described in step 5. The algorithm is executed symmetrically on every computing node involved in the simulation process as follows:

(1) The number of the wind turbines to be simulated is stored in a user defined integer array. Also, the locations and the geometric parameters of these wind turbines are stored in another user defined double precision array.
(2) For the assigned computational mesh partition, the number of the local mesh cells and their list are obtained.
(3) A search operation is performed on the assigned computational mesh partition to find out the mesh cells, which are intersected by any of the cone volumes that represent the wind turbines.
(4) For each of the obtained "intersected" cells, the matching-turbine index, the cell-index and the cell-radius (*the radius from the center of the matching-turbine to the cell-center*) are stored in a local lookup table. Therefore, each computing node will have its own lookup table of the corresponding cells-data to the different matching-turbines.
(5) The following pseudo code is executed every iteration of the flow field solution until convergence is reached (as described in Sec. 2.1).

Acquire *the local lookup table of the cells-data* (*obtained in step*4).
For *each of the cells within the current lookup table*
  Compute *the upcoming reference velocity as discussed in the previous subsection.*
  If *the current cell within the nacelle zone of the corresponding matching-turbine* **then**
    Compute *the normal surficial force exerted by the nacelle on the flow.*
  Else
    Call *the user defined subroutine of the improved BEM theory* [***WT index, the current cell-radius***, ***the reference velocity of***

the current cell *to compute the induction factors (axial and tangential) and the forces that act on the current blade element.*

End If

Compute *the source term components, Eq.* (7)*, corresponding to the current mesh cell in order to update the RHS of the different components of the momentum equation.*

Compute *the current contribution to thrust force and power of the current matching-turbine.*

End For

(6) After the convergence of the flow field solution, collect and sum up all contributions of thrust force and power of every WT under consideration.

In this manner, the interaction between the wind turbines and the terrain of the farm is computed iteratively until convergence.

3. Simulation Setup

The problem under consideration is often very large, tightly-coupled, and multi-scale. The need to transcend Moore's law through parallel computing on clusters, grids and scalable parallel systems has augmented in recent years. Parallel solution approaches based on parallel mesh-decomposition techniques are required to exploit these parallel architectures for large scale CFD problems. While standard clusters and grids can address a sub-class of these problems [Hussein and El-Shishiny (2007)], an entire range of complex, interdisciplinary, multi-scale, turbulent flow problems requires ultra-scalable HPC architectures. These systems are large, have tight-coupled processors with high bandwidth and low latency interconnects as well as an optimized message-passing library, such as message passing interface (MPI) [Blue Gene Literature (2009)]. The IBM Blue Gene/L HPC system is used in this research work, as it is an ultra-scale computer that has been very effective in addressing these classes of challenging CFD problems.

Code_Saturne version 1.4 [Archambeau *et al.* (2004); Code_Saturne (2009)] is used in the present work as the CFD core simulation engine, which was optimized for Blue Gene supercomputers [Fournier *et al.* (2011)]. On the other hand, an efficient parallel method for implementing VBM was developed, as described in Sec. 2.3, using the data structures of the Code_Saturne and integrated with it as user subroutines. The preprocessor components of Code_Saturne were compiled to work on the Blue Gene/L front-end machine, which is running Linux, and linked to the METIS library as a powerful partitioning tool [METIS (2010)]. Computational meshes were generated using Gambit 2.2.3 [Fluent (2009)] and exported in its neutral format, which can be imported easily by Code_Saturne.

The Blue Gene/L contains a single or multiple racks, and each rack has 1024 two-core-CPUs [Blue Gene Literature (2009)]. Blocks of CPUs can be requested by users and booted in one of two modes; coprocessor mode (CO) and virtual Node mode (VN). In CO mode, one CPU core handles all MPI and external I/O and

the other core runs the user's code, and the user's code can access up to ∼500 MB RAM per task. On the other hand, in VN mode, both CPU cores handle their own MPI and external I/O and also run the user's code, and the user's code can access up to ∼244 MB RAM per task. Code_Saturne kernel was compiled to work on Blue Gene/L enabling MPI-IO, and the launching script was customized to fit the existing environment structure. In this manner, the MPIRUN command, within the launching script, not only includes the case executable code and its parameters, the allocated block ID, the number of utilized computing nodes, but also the mode of operation (CO or VN).

The accuracy of the simulation environment was verified first by simulating the flow in a 3-D diffuser with predefined inlet profiles, as one of the benchmark test cases [Test Cases (2010)] that are described technically by Cherry *et al.* [2006, 2008]. The computational mesh used has $212\times60\times180$ cells with $0.0001 < y^+ < 0.00375$ for the near wall cells. The mesh preprocessing and partitioning were performed on the Blue Gene/L front-end machine employing the METIS library [METIS (2010)] for efficient partitioning [Fournier *et al.* (2011)]. The steady state solution was reached after 10,000 iterations, and the numerical results, applying different turbulence models, were in good agreement with that of both [Cherry *et al.* (2008)] and [Test Cases (2010)].

4. Results and Discussion

The wind flow over micro-scale wind farm with rough flat terrain was simulated at the operating conditions of the Tjaereborg wind turbines installed in the farm [Tjaereborg WT Loads (1994); Operational Data for Tjaereborg WT (1990)]. The Tjaereborg rotor has a diameter of 61 m and consists of three blades composed of NACA 4412-43 aerofoil sections. For each blade, the chord length is 0.9 m at the tip, increasing linearly through the blade length of 29 m to 3.3 m at the hub. In addition, the blades are twisted 1° per 3 m, and the turbine hub height is 60 m. The tip speed is 70.7 m/s and the rotor solidity is 5.9%. The inlet turbulence intensity was set to 10% at the turbines' hub-height. This conditions were reached by setting the flat terrain roughness to $z_o = 0.003075997$ m according to Eq. (2) while the inlet velocity at hub-height was set to 10 m/s.

4.1. *Simulation of wind over a single Tjaereborg wind turbine installed on flat terrain micro-scale wind farm*

4.1.1. *Simulation results*

The computational domain extended 11 turbine diameters vertically, 10 turbine diameters laterally, 10 diameters upstream and 20 diameters downstream the turbine as shown in Fig. 4(a). The computational domain was discretized in the fashion shown in Fig. 4(b). The first computational node off the wall was placed at 0.1 m,

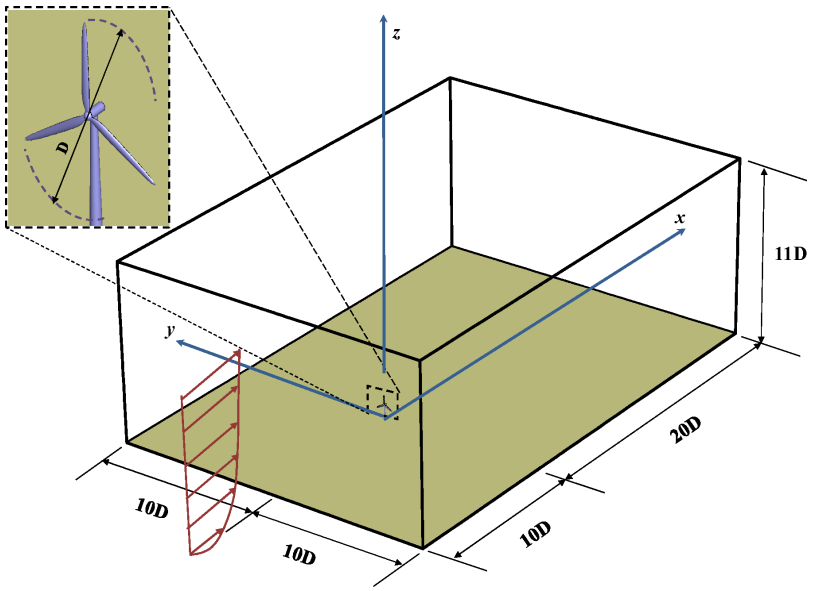

(a) Dimensions of the computational domain.

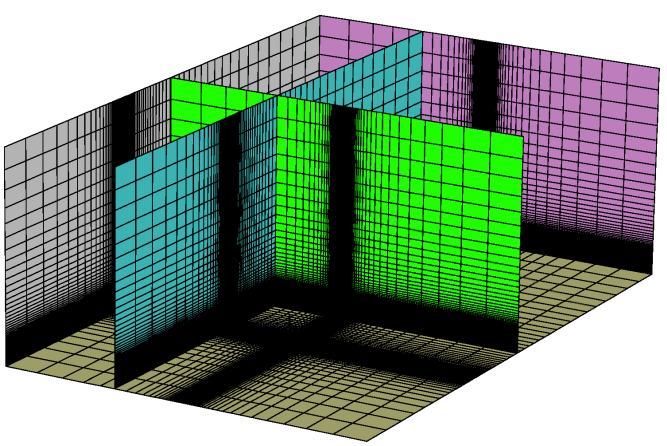

(b) Details of the computational mesh.

Fig. 4. Description of the computational domain, Tjaereborg WT installed on flat terrain, wind speed at hub-height = 10 m/s.

satisfying the condition of rough wall, while the minimum grid distance in the x-direction (before and after the turbine) was set to 0.5 m.

A grid dependency study was conducted to determine the sufficient number of points needed to represent each turbine blade and its impact on the overall mesh size. Figure 5(a) illustrates the variation of the hub-height velocity deficit at the rotor position ($x/D = 0$) and at a position ($x/D = 3$) downstream the turbine as

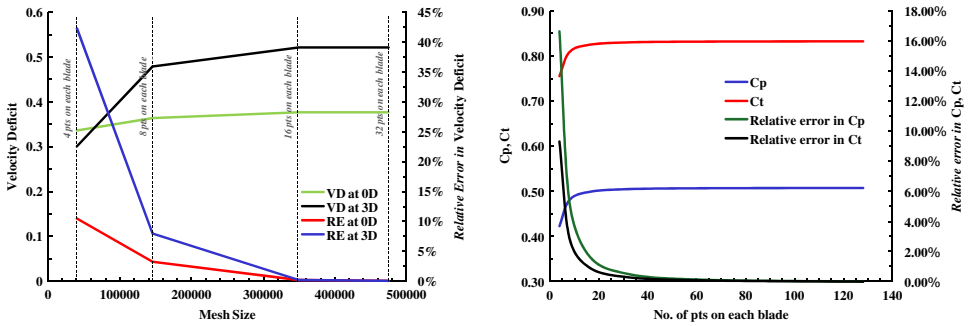

(a) Velocity deficit.

(b) Thrust and power coefficients.

Fig. 5. Grid dependency study for simulating wind over micro-scale wind farm contains a single Tjaereborg WT, wind speed at hub-height = 10 m/s.

a function of the number of points used to represent each turbine blade and the overall mesh size. Here, the relative error in the velocity deficit was computed with reference to the grid independent solution. As shown, the grid-independent solution was reached using 32 points to represent each turbine blade. This was confirmed from the power coefficient and the thrust coefficient as shown in Fig. 5(b). The associated overall computational mesh size was 4,46,250 mesh cells, keeping the overall quality of the mesh. The predicted velocity deficit is in a good agreement with the measurement-supported correlation of Glauert [Burton *et al.* (2001)] while the predicted power and thrust coefficients are in a good agreement with the experimental data published in [Mikkelsen (2003)].

The axial velocity deficit downstream the rotor is computed using:

$$\Delta U = 1 - \left(\frac{U_{\text{axial}}(\text{with WT})}{U_{\text{axial}}(\text{without WT})} \right). \tag{11}$$

In this manner, the predicted axial velocity deficit, at hub height downstream the rotor, using the VBM is compared to that predicted using the constant loading ADM, Eq. (8), as shown in Fig. 6(a). The predicted velocity deficit using the VBM (including the nacelle) deviates clearly from that predicted using constant loading ADM. It is interesting to point out that, from this figure, the VBM predicts the wake of the WT to be extended $8D$ downstream while the constant loading ADM predicts the wake of the WT to be more than $14D$. The pressure and the turbulence intensity along the axis of the WT computed using the VBM are compared to that predicted using the ADM as shown in Figs. 6(b) and 6(c). The ADM underestimates both the pressure and the turbulence intensity change across the wind turbine.

The velocity profiles downstream the WT were also studied as shown in Fig. 7. In this figure, in the near wake region up to $x/D = 3$, the VBM predictions clearly deviate from that of the ADM then converge in the far wake region. It is interesting

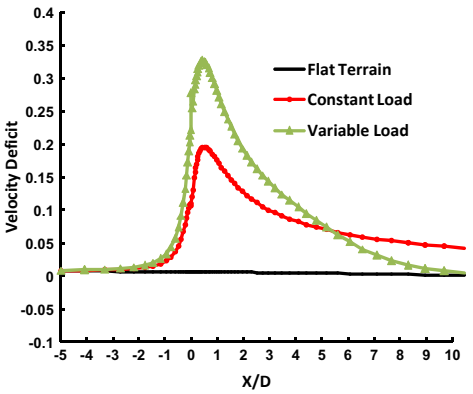

(a) Axial velocity deficit.

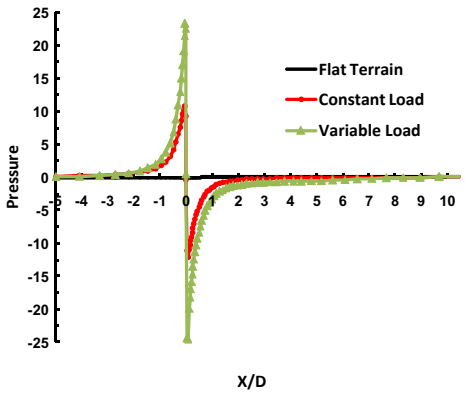

(b) Axial pressure.

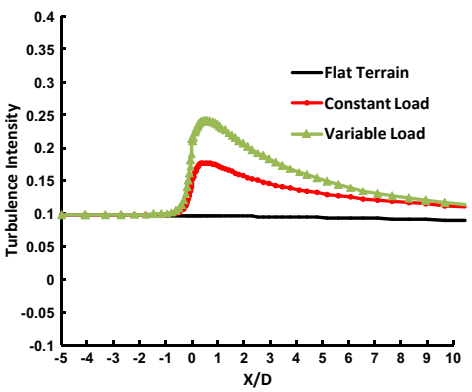

(c) Axial turbulence intensity.

Fig. 6. Wind parameters in the presence of Tjaereborg WT at $x/D = 0$, wind speed at hub-height $= 10\,\mathrm{m/s}$.

to point out that the deviations between the predictions of VBM and ADM derived mainly from considering the load variation on the WT blades, in both radius and azimuth directions, in VBM while approximating the wind loading as a constant along the different turbine blades in ADM. The wake region downstream the rotor is investigated using the velocity magnitude as depicted in Fig. 8 (for the two methods emphasizing the effect of modeling the rotor nacelle in the application of VBM). The velocity field and the wake region are illustrated in Fig. 9, demonstrating the size of the wake region.

The simulations were conducted to study the WT output power at different wind speed values. Figure 10(a) shows the variation of the predicted WT power as a function of the wind speed using VBM, in comparison with that predicted using standalone BEM [Burton *et al.* (2001)] and the experimental data published

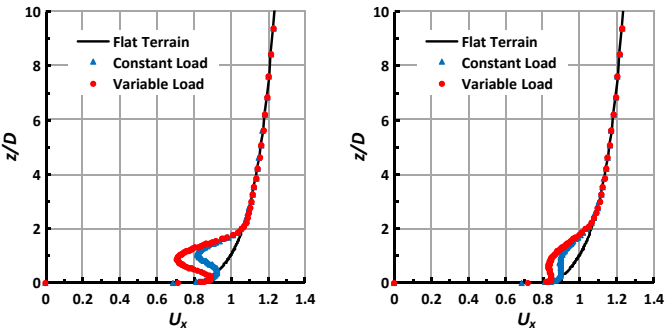

(a) $x/D = 1$.

(b) $x/D = 3$.

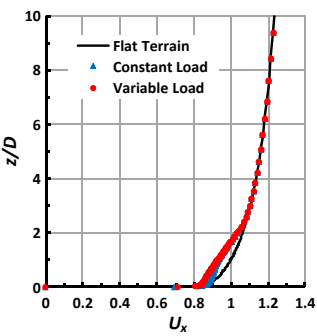

(c) $x/D = 5$.

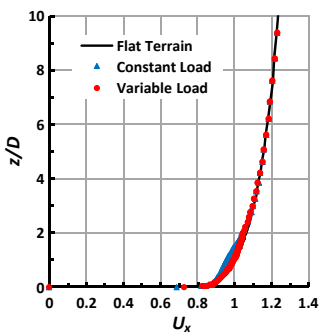

(d) $x/D = 10$.

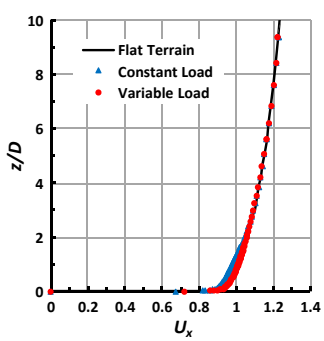

(e) $x/D = 20$.

Fig. 7. Velocity profiles downstream Tjaereborg WT, wind speed at hub-height = 10 m/s.

in [Mikkelsen (2003)]. Also, the variation of the predicted power coefficient with tip speed ratio is compared to that predicted using standalone BEM and the experimental data of [Mikkelsen (2003)] as depicted in Fig. 10(b). As shown, the predicted output power agrees well with BEM for wind speeds less than 15 m/s and in good agreement with the experimental data for the considered range of wind speeds.

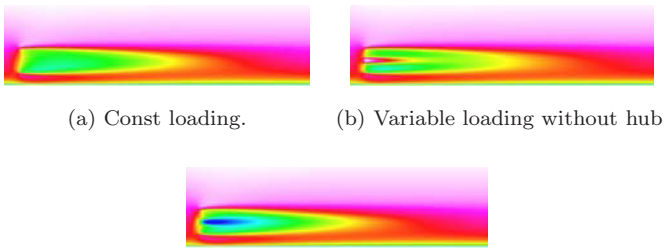

(a) Const loading. (b) Variable loading without hub.

(c) Variable loading with hub.

Fig. 8. Wake downstream Tjaereborg wind turbine, wind speed at hub-height = 10 m/s.

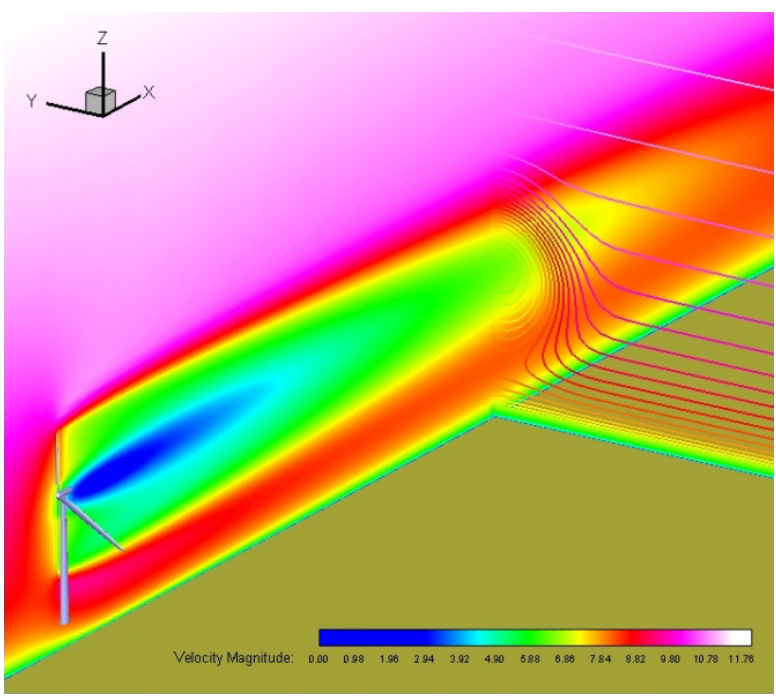

Fig. 9. Wake structure downstream Tjaereborg turbine installed on flat terrain, wind speed at hub-height = 10 m/s.

4.1.2. *Performance analysis of the integrated solver*

The performance of Code_Saturne "only" was studied first by simulating the flow over the wind farm without the turbine to be the baseline for further comparisons. This simulation was repeated using different numbers of processors, employing both CO and VN booting modes. The computing mesh was partitioned in the preprocessing phase on the Blue Gene/L front-end machine via Code_Saturne preprocessor, employing the METIS library to get the most efficient partitioning [Fournier *et al.*

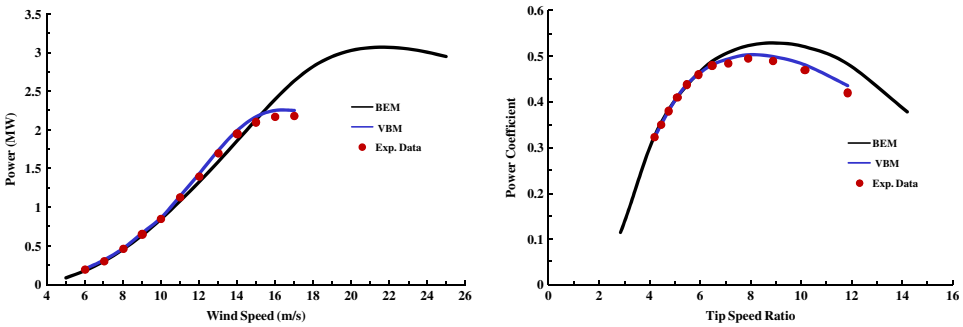

(a) Variation of output power with wind speed. (b) Variation of power coefficient with TSR.

Fig. 10. Computed performance of Tjaereborg wind turbine.

(2011)]. For the case of using 512 processors, the minimum partition size was 846 cells and the maximum partition size was 898 cells. The median of partition sizes was 870 and the standard deviation was 18.27, which prove the efficiency of the decomposition process.

The local-maximum-work-memory-used was examined for each case. The local-maximum-work-memory-used starts at 13 MB at 16 processors and declined exponentially to less than 2 MB at 1,024 processors. This gives a fair comparison between the scalability for both the CO and the VN modes, as the ceiling of the local-maximum-work-memory-used is below the 244 MB provided in the VN mode. The speedup of the computation was studied versus the number of processors used for both the CO and the VN booting modes. As shown in Fig. 11(a), the speedup exhibits ideal behavior up to 64 processors for both CO and VN modes then slightly deviates from the ideal behavior.

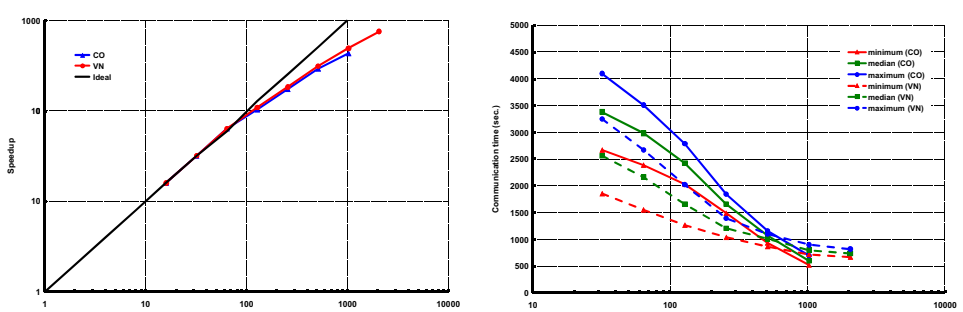

(a) Speedup of computations. (b) Communication time of computations.

Fig. 11. Performance analysis of the CFD solver for the simulation of wind flow over flat terrain "only."

To understand the observed deviation of the speedup from the ideal behavior, the communication time was studied for various cases to investigate the influence of increasing the number of processors on the intercommunication between them. Generally, the VN mode exhibits less communication time than that of the CO mode for the same number of CPUs as shown in Fig. 11(b). For both modes, the communication time decreases as the number of the utilized processors increasing, and the slope of these time curves also decreases. On the other hand, the trends of the communication time deduce that the intercommunication is not the reason of the slight deviation of the speedup from the ideal behavior. It appears that the deviation originates from the fact that, for a specific mesh size, there is no gain from further decomposition (*as the overheads of the decomposition process and the numerical issues balance the gain from increasing the number of the utilized processors*).

Next, the performance of the integrated CFD solver was studied for the wind over micro-scale flat terrain wind farm containing a single "Tjaereborg" wind turbine. The WT was simulated using the proposed VBM and the constant loading ADM. Simulations were performed on the same computational mesh depicted in Fig. 4. Figure 12(a) shows the speedup of the computations versus the number of the utilized processors in the CO mode. As shown, the speedup exhibits almost similar behavior like that of the flat terrain simulations. This proves the minimum overhead imposed on the Code_Saturne CFD solver by the VBM module. On the other hand, the computing time per iteration was studied for the integrated CFD solver versus the number of the utilized processors. As expected, for the cases of VBM, the integrated solver consumes more computing time, especially at lower number of processors used. By increasing the number of the utilized processors, the computing time for both VBM and ADM approaches that of the flat terrain without any WT. The speedup of the integrated CFD solver was also studied for both CO and VN

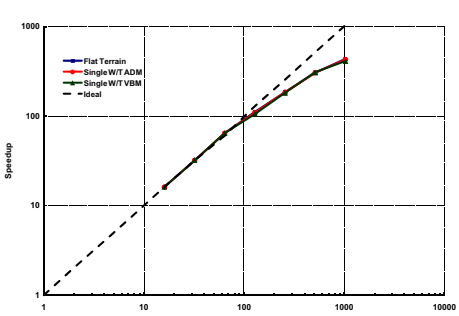

(a) Computations using VBM and ADM, CO BG/L booting mode.

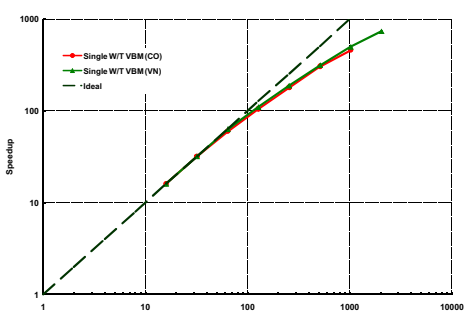

(b) Computations using VBM, CO and VN BG/L booting modes.

Fig. 12. Speedup of the integrated CFD solver for the wind flow simulation over micro-scale wind farm contains single Tjaereborg WT, wind speed at hub-height = 10 m/s.

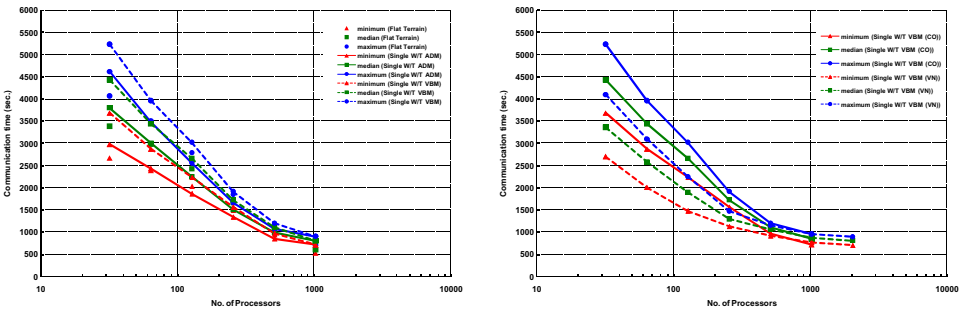

(a) Computations using VBM and ADM, CO BG/L booting mode.

(b) Computations using VBM, CO and VN BG/L booting modes.

Fig. 13. Communication time of the integrated CFD solver for the wind flow simulation over micro-scale wind farm contains single Tjaereborg WT, wind speed at hub-height = 10 m/s.

booting modes as shown in Fig. 12(b). As expected, the VN mode exhibits better performance, as there are no extensive I/O operations, and the maximum-work memory-used is below the ceiling value of the VN mode.

The intercommunication between the processors was studied as a function of the communication time for the computations of wind flow over a single WT installed on a flat terrain using both VBM and ADM, compared to that of the wind over flat terrain only. Figure 13(a) shows the communication time versus the number of utilized processors using the CO mode. As expected, the integrated Code_Saturne CFD solver consumes more communication time than that of the standalone Code_Saturne used to simulate the wind flow over flat terrain only. As the number of the utilized processors increases, the communication time of the integrated CFD solver approaches that of the standalone one. Finally, the communication time of the integrated CFD solver was studied versus the number of the utilized processors for both the CO and the VN booting modes. As shown in Fig. 13(b), the communication time of the CO mode significantly differs from that of the VN mode. This difference decreases as the number of processors increases and vanishes at 512 processors. Therefore, for similar simulation cases, the VN mode is more preferable than the CO mode at lower number of processors used.

4.2. *Simulation of wind over two-rows Tjaereborg wind turbines installed on flat terrain micro-scale wind farm*

4.2.1. *Simulation results*

The wind over two rows of Tjaereborg wind turbines installed on flat terrain was simulated for wind speed of 10 m/s at turbines hub-height. The terrain surface roughness was set to $z_o = 0.003075997$ m to keep the inlet hub-height turbulence intensity at 10%. The two rows were represented by two wind turbines simulated in a computational domain with periodic boundary conditions applied to its lateral sides.

The two wind turbines are installed 6 diameters apart in the longitudinal direction (x-direction) and 4 diameters apart in the lateral direction. The computational domain extended 11 diameters vertically, 2 diameters laterally from each turbine, 10 diameters upstream from the first turbine and 20 diameters downstream the second turbine and the computational domain was discretized in a fashion shown in Fig. 14(a), employing the recommendations drawn from the grid dependence study conducted in the previous subsection. The first computational node off the wall was placed at 0.1 m, satisfying the condition of rough wall, while the minimum grid distance in the x-direction (before and after each turbine) was set to 0.5 m. The overall mesh size is 8,50,000 cells. Figure 14(b) shows cross-sectional view through the wake of each turbine demonstrating the extension of the wake of each turbine via velocity magnitude contours.

The axial velocity deficit, Eq. (11), for each of the two rows, at hub height, was compared with that predicted for a single turbine, installed on flat terrain, and flat terrain only as shown in Fig. 15(a). The predicted velocity deficit for the first row follows that of the single turbine upstream the row and downstream the row up to $x/D = 3$ then starts to deviate clearly from the single turbine. For the second

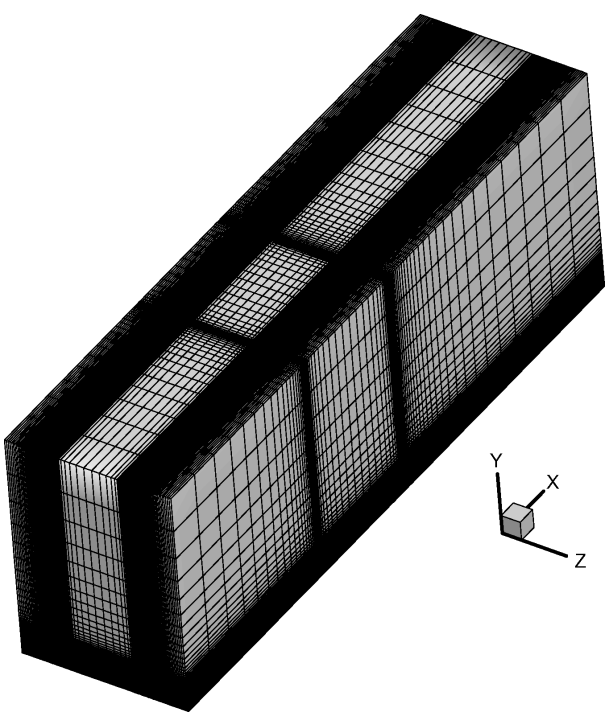

(a) Computational Mesh.

Fig. 14. Simulation of two rows Tjaereborg WTs installed on micro-scale wind farm using VBM, wind speed at hub-height = 10 m/s.

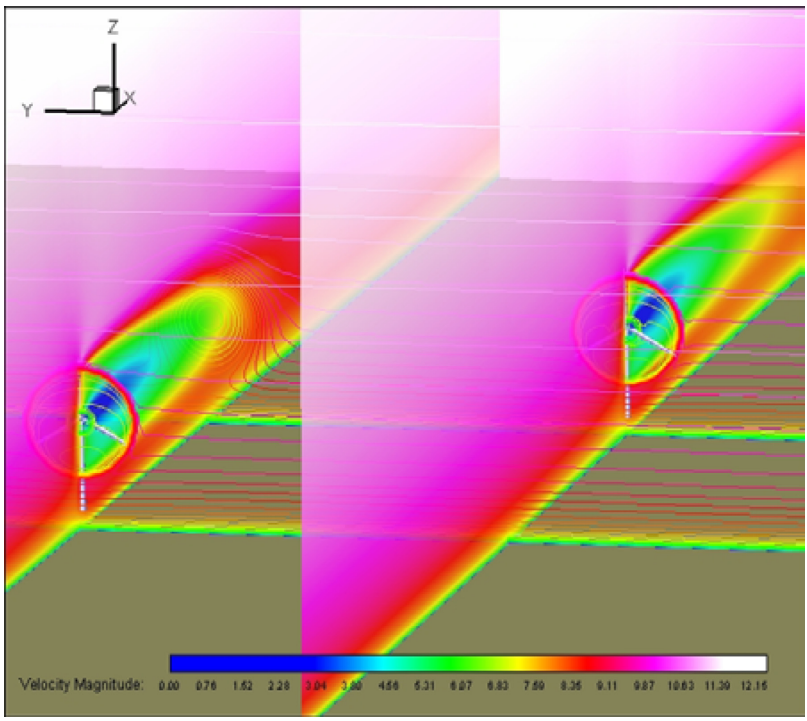

(b) Turbines wake representation via velocity contours.

Fig. 14. (*Continued*)

row, the predicted velocity deficit clearly deviates from that of the single turbine downstream the row. The pressure drop throughout both of the rows follows that of the single turbine as shown in Fig. 15(b). The turbulence intensity for both rows has the same velocity deficit behavior as shown in Fig. 15(c).

The velocity profiles downstream the wind turbines of the two rows were also studied as shown in Fig. 16 compared to that of the single turbine installed on flat terrain and flat terrain only. The profiles of the first row follow that of the single turbine installed on the flat terrain while the profiles of the second row clearly deviate in the near wake region up to $x/D = 3$.

4.2.2. *Performance analysis of the integrated solver*

The performance of the integrated CFD solver on the Blue Gene/L was studied in simulating the wind flow over two-rows micro-scale wind farm installed on flat terrain using different numbers of processors and employing the CO booting mode. The computing mesh was partitioned in the preprocessing phase on the front-end machine via Code_Saturne preprocessor employing the METIS library, aiming at getting the most efficient partitioning [Fournier *et al.* (2011)]. In case of using 512

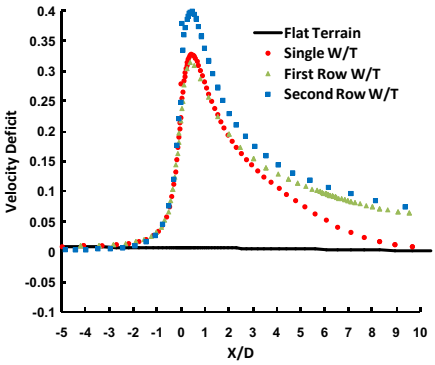

(a) Axial velocity deficit.

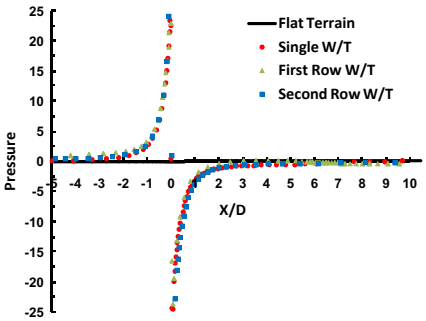

(b) Axial pressure.

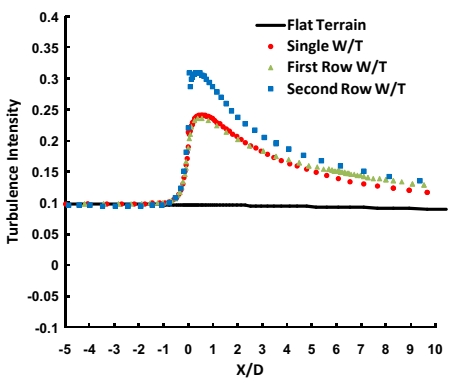

(c) Axial turbulence intensity.

Fig. 15. Wind parameters in the presence of two rows Tjaereborg WTs installed on micro-scale wind farm, wind speed at hub-height = 10 m/s.

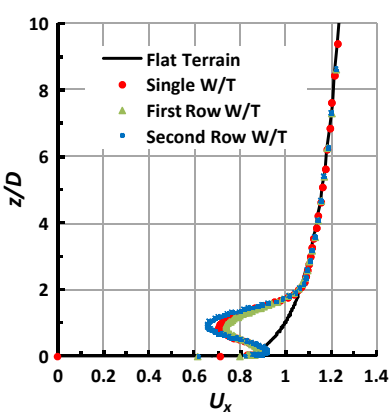

(a) $x/D = 1$.

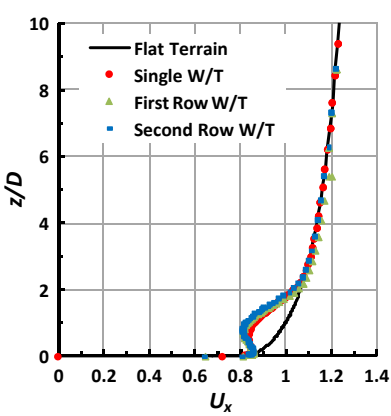

(b) $x/D = 3$.

Fig. 16. Velocity profiles downstream two rows Tjaereborg WTs installed on micro-scale wind farm, wind speed at hub-height = 10 m/s.

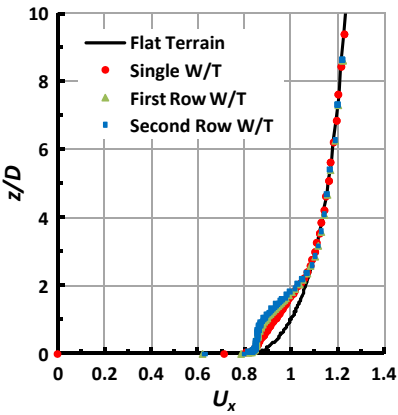

(c) $x/D = 5$.

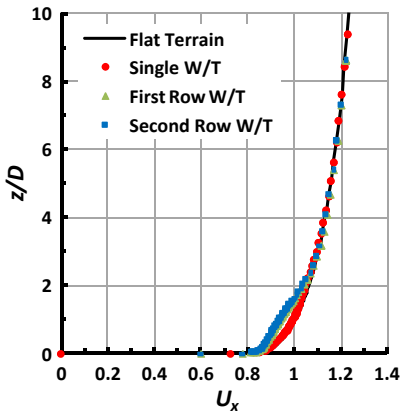

(d) $x/D = 10$.

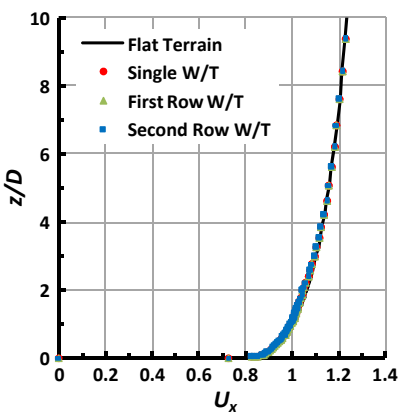

(e) $x/D = 20$.

Fig. 16. (*Continued*)

processors, the minimum partition size was 1,611 cells while the maximum partition size was 1,710 cells. The median was 1,661 and the standard deviation was 35.18, which proves the efficiency of the decomposition process.

The scalability of the integrated CFD solver was studied as shown in Fig. 17(a). The speedup of the computations was compared to that of the single wind turbine. It is interesting to point out that increasing the number of simulated wind turbines from one to two in addition to the overheads of applying the periodic boundary conditions did not lead to significant change in the speedup of the integrated CFD solver. This slight change in the speedup can be explained by studying the inter-communication between the processors represented by the communication time as shown in Fig. 17(b). For the current problem, the communication time is one order of magnitude above that of the simulation of wind over a single WT installed on

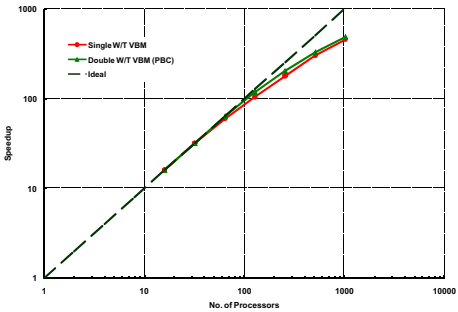

(a) Speedup versus the number of processors.

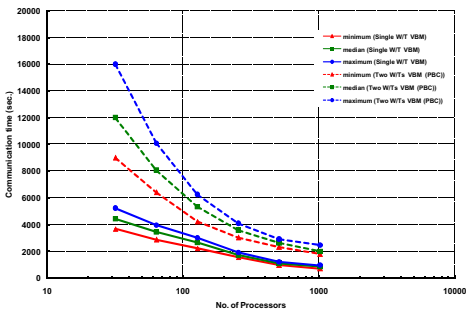

(b) Communication time versus the number of processors.

Fig. 17. Performance analysis of the integrated CFD solver for the wind flow simulation over two-rows Tjaereborg WTs installed on micro-scale wind farm, wind speed at hub-height = 10 m/s.

flat terrain. This increase in the communication time is originated from the difference in the computational mesh size and the application of the periodic boundary condition, in addition to the application of the VBM for two turbines instead of one.

5. Conclusions and Future Work

In this work, a computational framework for modeling and simulation of micro-scale (and early meso-scale) wind farms was proposed. This framework was formulated and implemented for the distributed memory, massively parallel high performance computing platforms like IBM Blue Gene/L supercomputer. The atmospheric boundary layer flow over the wind farms is modeled using the RANS equations along with the k–ε turbulence model. The wind turbines installed in the wind farm are modeled by VBM. This model considers the presence of the wind turbines' rotors implicitly through the source terms in the momentum equations. Code_Saturne version 1.4 was used in the present work as the CFD simulation engine, which was optimized for the usage of Blue Gene supercomputers. On the other hand, an efficient parallel algorithm for implementing VBM was developed using the data structures of the Code_Saturne and integrated with it as a user subroutine. The accuracy and performance of the proposed framework were confirmed through several simulations of wind over micro-scale wind farms. It is interesting to point out that the performance of the framework is improved for larger sizes of computational meshes. In addition, results showed that there is no degradation in the performance of the CFD simulation engine due to the integration with the proposed VBM algorithm. The proposed framework is capable of simulating micro-scale (or early meso-scale) wind farms with several wind turbines and/or complex terrain. The whole framework is ported and optimized to run also on a Grid computing platform, EUMEDGRID e-Infrastructure through the grid interface provided by

the Egyptian Universities Network, to simulate real-life cases for decision-making purposes.

As a future work, real cases of micro-scale wind farms with complex terrain will be simulated considering one of the hybrid RANS/large Eddy simulation (LES) methods. On the other hand, multi-scale numerical modeling will be considered to integrate meso-scale numerical weather prediction systems with CFD solvers at the micro-scale level. Finally, the developed framework will be integrated with an optimization engine to optimize the positioning of the wind turbines within a micro-scale wind farm, in order to maximize their power.

Acknowledgments

This work is part of an R&D project conducted at the IBM Center for Advanced Studies (CAS) in Cairo. The authors would like to thank Ahmed Sayed and Ali El-Moursy, IBM Centre for Advanced Studies in Cairo, for fruitful discussions. Special thanks go to the Code_Saturne Support Team (saturne-support@edf.fr), and Fred Mintzer and David Singer, IBM TJ Watson Research Centre, for their continuous support for the use of the Watson Blue Gene/L "BGD" for this work.

References

Ammara, I., Leclerc, C. and Masson, C. [2002] "A viscous three-dimensional differential/actuator disc method for the analysis of wind farms," *ASME J. Sol. Energy Eng.* **124**(4), 345–356, doi:10.1115/1.1510870.

Archambeau, F., Mechitoua, N. and Sakiz, M. [2004] "A finite volume method for the computation of turbulent incompressible flows-industrial applications," *Int. J. Finite Volumes* **1**(1), 1–61, available at http://www.citeulike.org/group/8515/article/4016818.

Ayotte, K. W. and Hughes, D. E. [2004] "Observations of boundary-layer wind-tunnel flow over isolated ridges of varying steepness and roughness," *Bound.-Layer Meteorol.* **112**(3), 525–556, doi:10.1023/B:BOUN.0000030663.13477.51.

Benjanirat, S., Sankar, L. N. and Xu, G. [2003] "Evaluation of turbulence models for the prediction of wind turbine aerodynamics," *AIAA Paper* 2003-0517. Available at http://soliton.ae.gatech.edu/people/lsankar/NREL/Reno.paper.2003.pdf.

Blue Gene Literature: Analyst reports, deep computing, IBM systems, [Online last accessed 2009] Available at http://www-03.ibm.com/systems/deepcomputing/bluegene/bg_lit_ar.html.

Burton, T., Sharpe, D., Jenkins, N. and Bossanyi, E. [2001] *Wind Energy: Handbook* (John Wiley & Sons, LTD., UK) ISBN 0471489972.

Cabezón, D., Sanz, J., Martí, I. and Crespo, A. [2009] "CFD modelling of the interaction between the surface boundary layer and rotor wake," *Proc. EWEC 2009*, Parc Chanot, Marsseille, France.

Cherry, E. M., Elkins, C. G. and Eaton, J. K. [2006] "Separated flow in a three-dimensional diffuser: Preliminary validation," *Proc. Annual Research Brief 2006*, Center for Turbulence Research, Stanford University, pp. 31–40.

Cherry, E. M., Elkins, C. G. and Eaton, J. K. [2008] "Geometric sensitivity of three dimensional separated flows," *Heat Fluid Flow* **29**(3), 803–811, doi:10.1016/j.ijheatfluidflow.2008.01.018.

Code_Saturne EDF's general purpose computational fluid dynamics (CFD) software. [Online last accessed 2010]. Available at http://research.edf.com/the-end-offers/research-and-development/softwares/code-saturne-107008.html.

Crespo, A., Hernandez, J. and Frandsen, S. [1999] "Survey of modelling methods for wind turbine wakes and wind farms," *Wind Energy* **2**(1), 1–24, doi:10.1002/(SICI)1099-1824(199901/03)2:1<1::AID-WE16> 3.0.CO;2-7.

Dobrev, I., Massouh, F. and Rapin, M. [2007] "Actuator surface hybrid model," *J. Phys. Conf. Ser. The Science of Making Torque from Wind* (*2nd Conference*), **75**, 012019. doi:10.1088/1742-6596/75/1/012019.

Duque, E. P. N., Van Dam, C. P. and Hughes, S. [1999] "Navier–Stokes simulations of the NREL combined experiment phase II rotor," *AIAA Paper* 97-0037.

Ekaterinaris, J. A. [1997] "Numerical simulation of incompressible two-bladed rotor flow field," *AIAA Paper* 97-0398, EUMEDGRID Support Project (2011), FP7-INFRASTRUCTURES-2009-1-SA-246589, http://www.eumedgrid.eu/

El-Kasmi, A. and Masson, C. [2008] "An extended k-epsilon model for turbulent flow through horizontal-axis wind turbines," *Wind Eng. Ind. Aerodyn.* **96**(1), 103–122, doi:10.1016/j.jweia.2007.03.007.

Fournier, Y., Bonelle, J., Moulinec, C., Shang, Z., Sunderland, A. G. and Uribe, J. [2011] "Optimizing Code_Saturne computations on Petascale systems," *Comput. Fluid.* **45**(1), 103–108, doi:10.1016/j.compfluid.2011.01.028.

Gambit User's Guide Version 2.2.3, FLUENT Software, FLUENT [Online last accessed 2009] Available at http://www.fluent.com/.

Geometric and Operational Data for the Tjaereborg Wind Turbine [1990] *Techinical Report*, VK-184, Department of Fluid Mechanics, DTH, DK 2800 Lyngby, p. 8.

Hansen, M. O. L. [2003] *Aerodynamics of Wind Turbines* (James & James, London) ISBN: 1902916069.

Hargreaves, D. M. and Wright, N. G. [2007] "On the use of the *k*-epsilon model in commercial CFD software to model the neutral atmospheric boundary layer," *Wind Eng. Ind. Aerodyn.* **95**(5), 355–369, doi:10.1016/j.jweia.2006.08.002.

Hussein, A. S. and El-Shishiny, H. [2009] "Influences of wind flow over heritage sites: A case study of the wind environment over the Giza plateau in Egypt," *Environ. Model. Software* **24**(3), 389–410, doi:10.1016/j.envsoft.2008.08.002.

Hussein, A. S. and El-Shishiny, H. [2007] "Modeling and simulation of low speed wind over the Great Sphinx," *Proceedings of 2007 IEEE Symposium of Computers and Communications* (*ISCC'07*), pp. 1027–1034, doi:10.1109/ISCC.2007.4381500.

Ingram, G. [2005] *Wind Turbine Blade Analysis Using the Blade Element Momentum Method*, School of Engineering, Durham University.

Ivanell, S. A. [2009] "Numerical computations of wind turbine wakes," *Technical Report*, Linne' Flow Centre, Department of Mechanics, Royal Institute of Technology, SE-100 44 Stockholm, Sweden.

Jackson, P. S. and Hunt, J. C. R. [1975] "Turbulent wind flow over a low hill," *Q. J. R. Meteorol. Soc.* **101**(430), 929–995, doi:10.1002/qj.49710143015.

Jimenez, A., Crespo, A., Migoya, E. and Garcia, J. [2007] "Advances in large-eddy simulations of a wind turbine wake," *J. Phys. Conf. Ser. The Science of Making Torque from Wind* **75**, 012041, doi:10.1088/1742-6596/75/1/012041.

Landberg, L., Myllerup, L., Rathmann, O., Petersen, E. L., Jørgensen, B. H., Badger, J. and Mortensen, N. G. [2003] "Wind resource estimation — an overview," *Wind Energy* **6**(3), 261–271, doi:10.1002/we.94.

Lanzafame, R. and Messina, M. [2007] "Fluid dynamics wind turbine design: Critical analysis, optimization and application of BEM theory," *Renewable Energy* **32**, 2291–2305, doi:10.1016/j.renene.2006.12.010.

Lissaman, P. B. S., Foster, D. R., Rumbaugh, J. H. and Boulder, C. [1989] "Technical description of AVENU," *Proc. Annual Meeting of American Solar Energy Society*, Denver, CA, USA, pp. 290–295.

Madsen, H. A. [1982] "The actuator cylinder: A flow model for vertical axis wind turbines," *Technical Report*, Aalborg University Center, Institute of Industrial Construction and Energy Technology, Aalborg, Denmark.

Makridis, A. and Chick, J. [2009] "CFD modeling of the wake interactions of two wind turbines on a Gaussian hill," *Proc. EACWE 5*, Florence, Italy.

Mandas, M., Cambuli, F. and Carcangiu, C. E. [2006] "Numerical prediction of horizontal axis wind turbine flow," *Proc. EWEC 2006*, Athens, Greece.

Manwell, J. F., McGowan, J. G. and Royers, A. L. [2002] *Wind Energy Explained* (Wiley, UK) ISBN: 0471499722, doi:10.1002/0470846127.fmatter_indsub.

Mason, P. J. and Sykes, R. I. [1979] "Three-dimensional numerical integrations of the Navier–Stokes for flow over surface-mounted obstacles," *Fluid Mech.* **91**(3), 433–450, doi:10.1017/S0022112079000240.

Masson, C., Ammara, I. and Paraschvoiu, I. [1997] "An aerodynamic method for the analysis of isolated horizontal axis wind turbines," *Int. J. Rotat. Mach.* **3**(1), 21–32, doi:10.1155/S1023621X97000031.

Masson, C., Smaili, A. and Leclerc, C. [2001] "Aerodynamic analysis of HAWTs operating in unsteady conditions," *Wind Energy* **4**(1), 1–22, doi:10.1002/we.43.

Menter, F. R. [1993] "Zonal two equation k-ω turbulence models for aerodynamic flows," *AIAA Paper* 93-2906.

Mikkelsen, R. [2003] *Actuator Disc Methods Applied to Wind Turbines*, Ph.D. Thesis, Department of Mechanical Engineering, Technical University of Denmark.

Palma, J. M. L. M., Castro, F. A., Ribeiro, L. F., Rodrigues, A. H. and Pinto, A. P. [2008] "Linear and nonlinear models in wind resource assessment and wind turbine micro-siting in complex terrain," *Wind Eng. Ind. Aerodyn.* **96**(12), 2308–2326, doi:10.1016/j.jweia.2008.03.012.

Rajagopalan, R. G. and Fanucci, J. B. [1985] "Finite difference model for the vertical axis wind turbines," *J. Propul. Power* **1**, 432–436.

Şahin, A. D. [2004] "Progress and recent trends in wind energy," *Progr. Energy Combust. Sci.* **30**(5), 501–543, doi:10.1016/j.pecs.2004.04.001.

Sanderse, B., van der Pijl, S. P. and Koren, B. [2011] "Review of CFD for wind-turbine wake aerodynamics," *Technical Report* 1386-3703, Department of Modelling, Analysis and Computing (MAC), doi:10.1002/we.458.

Sandström, S. [1994] "WASP-a comparison between model simulations and measurements," *Wind Energy Report WE 94:2*, Department of Meteorology, Uppsala University, Sweden.

Serial graph partitioning and fill-reducing matrix ordering, METIS, Karypis Lab., [Online last accessed 2010] Available at http://glaros.dtc.umn.edu/gkhome/metis/metis/overview.

Sørensen, J. and Shen, W. [2002] "Numerical modeling of wind turbine wakes," *J. Fluid Eng.* **124**(2), 393–399, doi:10.1115/1.1471361.

Sørensen, J. N. and Myken, A. [1992] "Unsteady actuator disc model for horizontal axis wind turbines," *Wind Eng. Ind. Aerodyn.* **39**(1–3), 139–149, doi:10.1016/0167-6105(92)90540-Q.

Sørensen, J. N., Mikkelsen, R. and Troldborg, N. [2007] "Simulation and modelling of turbulence in wind farms," *Proc. EWEC 2007*, European Wind Energy Association, Milan, Italy.

Sørensen, N. N. [1995] *General Purpose Flow Solver Applied to Flow over Hills*. Ph.D. Thesis Risø-R-827, Wind Energy Research, Technical University of Denmark.

Sørensen, N. N. and Michelsen, J. A. [2000] "Aerodynamics predictions for the unsteady aerodynamics experiment phase II rotor at the National Renewable Energy Laboratory," *AIAA Paper* 2000-0037.

Sumner, J., Watters, C. S. and Masson, C. [2010] "CFD in wind energy: The virtual, multiscale wind tunnel," *Energies* **3**, 989–1013, doi:10.3390/en3050989.

Test Cases, Code_Saturne TWiki, The University of Manchester, [Online last accessed 2010] Available at saturne.cfdtm.org.

The Tjaereborg Wind Turbine Loads during normal operation mode [1994] *Technical Report*, EP94/456, WEGA-I Measurement Project, ELSAMPROJEKT A/S, Power Station Engineering.

Troen, I. and Petersen, E. L. [1989] "European wind atlas," *Technical Report*, Risø National Laboratory, Denmark.

Troldborg, N., Sørensen, J. and Mikkelsen, R. [2007] "Actuator line simulation of wake of wind turbine operating in turbulent inflow," *J. Phys. Conf. Ser. The Science of Making Torque from Wind*, **75**, 012063, doi:10.1088/1742-6596/75/1/012063.

Vermeer, L. J., Sørensen, J. N. and Crespo, A. [2003] "Wind turbine wake aerodynamics," *Prog. Aerosp. Sci.* **39**(6–7), 467–510, doi:10.1016/S0376-0421(03)00078-2.

Wind Energy Annual Report [2007] International Energy Agency (IEA). *Wind Resource Assessment Handbook: Fundamentals for Conducting a Successful Monitoring Program* [1997] AWS Scientific Inc., NREL Subcontract N. TAT-5-15283-01, National Renewable Energy Laboratory.

Xu, G. and Sankar, L. N. [1999] "Computational study of HAWT," *AIAA Paper* 1999-0042, doi:10.1115/1.556278.

Xu, G. and Sankar, L. N. [2000] "Effects of transition, turbulence and yaw on the performance of HAWT," *AIAA Paper* 2000-0048.

Yang, Z., Sankar, L. N., Smith, M. and Bauchau, O. [2000] "Recent improvements to a hybrid method for rotors in forward flight," *Proc. AIAA Conference*, Reno, USA.

Zahle, F. and Sørensen, N. N. [2007] "On the influence of far-wake resolution on wind turbine flow simulations," *J. Phys. Conf. Ser. The Science of Making Torque from Wind* **75,** 012042. doi:10.1088/1742-6596/75/1/012042.

Zori, L. A. J. and Rajagopalan, R. G. [1995] "Navier–Stokes calculation of rotor-airframe interaction in forward flight," *J. Am. Helicopter Soc.* **40**(57), 11, doi:10.4050/JAHS.40.57.